Inorganic Chemistry

Article

Combined Experimental/Theoretical Study on the Luminescent Properties of Homoleptic/Heteroleptic Erbium(III) Anilate-Based 2D Coordination Polymers

Suchithra Ashoka Sahadevan, Fabio Manna, Alexandre Abhervé, Mariangela Oggianu, Noemi Monni, Valentina Mameli, Daniela Marongiu, Francesco Quochi, Frédéric Gendron, Boris Le Guennic, Narcis Avarvari,* and Maria Laura Mercuri*

Cite This: https://doi.org/10.1021/acs.inorgchem.1c02386

Read Online

ACCESS | Metrics & More | Article Recommendations | Supporting Information

ABSTRACT: The synthesis, structural and photophysical characterization, and theoretical studies on homo/heteroleptic neutral 2D-layered coordination polymers (CPs), obtained by combining the Er^{III} ion with chlorocyananilate (ClCNAn) and/or tetrafluoroterephthalate (F_4BDC) linkers, are herein reported. The structure of the heteroleptic Er^{III}-based CP, formulated as $[Er_2(ClCNAn)_2(F_4BDC)(DMSO)_6]_n$ (**1**) is also reported. **1** crystallizes in the triclinic $P\bar{1}$ space group, and the structure consists of neutral 2D layers formed by Er^{III} ions linked through the two linkers oriented in such a way that the neighboring 2D layers are eclipsed along the *a* axis, leading to parallelogram-like cavities. Photophysical measurements highlight the prominent role of chlorocyananilate linkers as optical antennas toward lanthanide ions, while wave-function-theory analysis supports the experimental findings, providing evidence for the effect of ligand substitution on the luminescence properties of homo/heteroleptic 2D CPs.
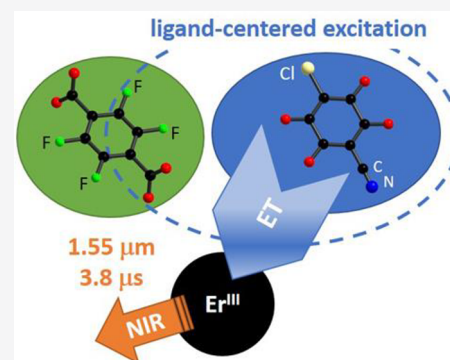

1. INTRODUCTION

Lanthanide coordination polymers (Ln-CPs) and metal–organic frameworks (Ln-MOFs), built by the self-assembly of Ln^{III} metal ions and conjugated organic linkers, have been extensively studied in recent years because of their intriguing structural topologies, optical properties, and several applications in various fields such as sensing, data storage, molecular spintronics and electronics, telecommunications, bioimaging, etc.[1–4] By proper tailoring of the coordination environment around the Ln^{III} metal ions, through (i) the various coordination modes of organic linkers and (ii) a selection of linkers with high absorptivity, thus acting as suitable *antennas* for sensitizing Ln ions, interesting supramolecular frameworks with peculiar luminescent properties[5,6] have been obtained. Some of the widely explored organic linkers behaving as valuable antennas are ligands with functional groups such as pyridyl, carboxylate derivatives, β-diketonates, etc.[6–11] A major drawback in the case of near-IR (NIR)-emitting complexes is nonradiative deactivation due to C–H, N–H, and O–H vibrations from ligands/solvents in close vicinity to Ln^{III} ions, which significantly quenches the luminescence. To overcome this issue, fluorinated ligands are often used, which reduce the fluorescence quenching effects of the overtones of C–H vibrations by considering low-frequency C–F vibrations.[12,13] In this context, 2,3,5,6-tetrafluoroterephthalic acid (F_4BDC) is a valuable ligand for the construction of multidimensional Ln-CPs and also for its

versatile and multidentate coordination modes to Ln ions through carboxyl O atoms.[14,15] On the other hand, CPs based on 3,5-disubstituted-2,6-dihydroxy-1,4-benzoquinone, commonly called anilates, have been widely studied over the past decade.[16–19] Anilates are excellent building blocks for the construction of layered mono/multifunctional materials showing magnetic,[20–25] conducting,[26–29] and luminescent properties.[30–32] Among them, the first example of a heterosubstituted anilate, the chlorocyananilate ligand (3-chloro-6-cyano-2,5-dihydroxybenzoquinone, $ClCNAn^{2-}$), is an interesting *antenna* linker for the construction of Ln-CPs because of the absence of IR quenchers in its molecular structure.[33] The ability of $ClCNAn^{2-}$ as an antenna toward NIR-emitting Ln^{III} ions was studied by some of us in both bulk-sized 2D CPs, formulated as $[Ln_2(ClCNAn)_3(DMF)_6]_n \cdot (DCM)_x$ (Ln = Yb, Nd, and Er; DMF = *N,N*-dimethylformamide; DCM = dichloromethane), and their related 2D ultrathin nanosheets obtained via solvent-assisted exfoliation methods by the top-down approach.[30]

A

Scheme 1. General Synthetic Procedure for the Synthesis of Hetero/Homoleptic Compounds[a]
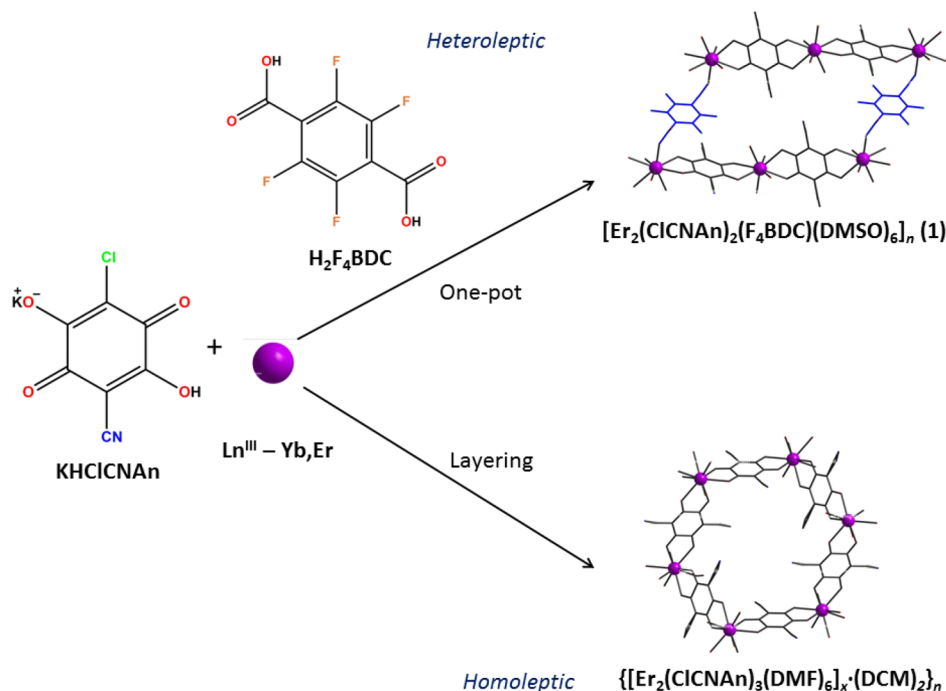
[a]The F_4BDC^{2-} linker in the heteroleptic compound is highlighted in blue.

A promising synthetic strategy to tune the structure and photophysical properties of Ln-CPs is the use of a suitable combination of mixed ligands[34] to provide heteroleptic CPs, despite the fact that these mixed-ligand materials are scarcely studied,[35] probably because of synthetic issues. The first ligand acts as an antenna to sensitize Ln^{III} emission, while the second ligand works as an ancillary bridging ligand for the construction of multidimensional networks. Very recently, some of us reported on the fabrication of robust and crystalline nanosheets of mixed-linker (heteroleptic) 2D CPs based on Yb^{III} and anilate/carboxylate derivatives, formulated as $[Yb_4(ClCNAn)_5(DOBDC)_1(DMSO)_{10}]_n \cdot (DMSO)_2$ (DOBDC = 2,5-dihydroxybenzene-1,4-dicarboxylic acid; DMSO = dimethyl sulfoxide) and $[Yb_2(ClCNAn)_2(F_4BDC)-(DMSO)_6]_n$, as innovative sensing nanoplatforms for nitroaromatics, paving the way to environmental sensing applications.[31] A CP built by the combination of mixed ligands, formulated as $Nd(F_4BDC)_{1.5}(phen)(H_2O)]_n$ (phen = 1,10-phenanthroline), is also reported as a sensor for the detection of explosives such as cyclotetramethylenetetranitramine.[36] In this material, both linkers contribute to the stability of the structure because of the rigidity of the ligands.

To the best of our knowledge, there are only a few heteroleptic CPs based on anilate/dicarboxylate ligands and NIR-emitting lanthanides. We report herein on the synthesis, structural characterization, and luminescent properties of a novel heteroleptic neutral 2D CP, formulated as $[Er_2(ClCNAn)_2(F_4BDC)(DMSO)_6]_n$ (**1**), prepared by combining Er^{III} ions with ClCNAn/F_4BDC linkers, via a one-pot synthetic strategy. The role of the linkers in the sensitization and emission processes of Er^{III} is studied spectroscopically and compared to previous findings on homoleptic ytterbium(III) and erbium(III) chlorocyananilate-based 2D CPs. A theoretical study based on wave-function-theory (WFT) analysis is performed to gain deeper insights into the luminescent

properties of the CPs and to shed light on the sensitization mechanism of the NIR-emitting Ln ions.

2. RESULTS AND DISCUSSION

2.1. Synthesis and Crystal Structure. 1 is formed by combining Er^{III} salt with both of the linkers ClCNAn^{2-} and F_4BDC^{2-} by an one-pot synthetic reaction in water. The obtained red solid is recrystallized in DMSO, affording, after several weeks, red single crystals suitable for X-ray analysis. The synthesis of 2D hetero/homoleptic CPs with Ln^{III} = Er and Yb, discussed in the text, is shown in Scheme 1. The molecular structures and luminescent properties of homoleptic and heteroleptic Yb-CPs were already reported.[30,31]

Single-crystal X-ray analysis reveals that **1** crystallizes in the triclinic $P\bar{1}$ space group. In the structure, the Er^{III} ions are connected through mixed linkers ClCNAn^{2-} and F_4BDC^{2-}, leading to a neutral 2D-layered CP. The asymmetric unit consists of one Er^{III} ion, two half-molecules of ClCNAn^{2-}, one half-molecule of F_4BDC, and three molecules of DMSO. As is generally seen in ClCNAn-based CPs,[21,30,31,37] chloro and cyano substituents are disordered and occupy two positions with an occupancy factor of 0.5 each. The two ligands exhibit different coordination modes around the metal ion, where ClCNAn^{2-} is coordinated to the Er^{III} ions in the usual bidentate mode, whereas F_4BDC^{2-} coordinates in a monodentate manner.

Each Er ion is eight-coordinated by four O atoms from ClCNAn^{2-}, one O atom from F_4BDC^{2-}, and three O atoms from a coordinated DMSO solvent molecule (Figure 1a), forming a ErO$_8$ polyhedron with distorted trigonal-dodecahedral geometry (Figure S1). The Er−O bond distances and O−Er−O bond angles range between 2.218(2) and 2.431(2) Å and between 65.54(8) and 145.29(8)°, respectively. As shown in Figure 1b, the ClCNAn^{2-} ligands bridge two Er^{III} ions in a bis-1,2-bidentate manner, forming a 1D chain along the c axis. The second ligand, F_4BDC^{2-}, acts as a bridge between neighboring
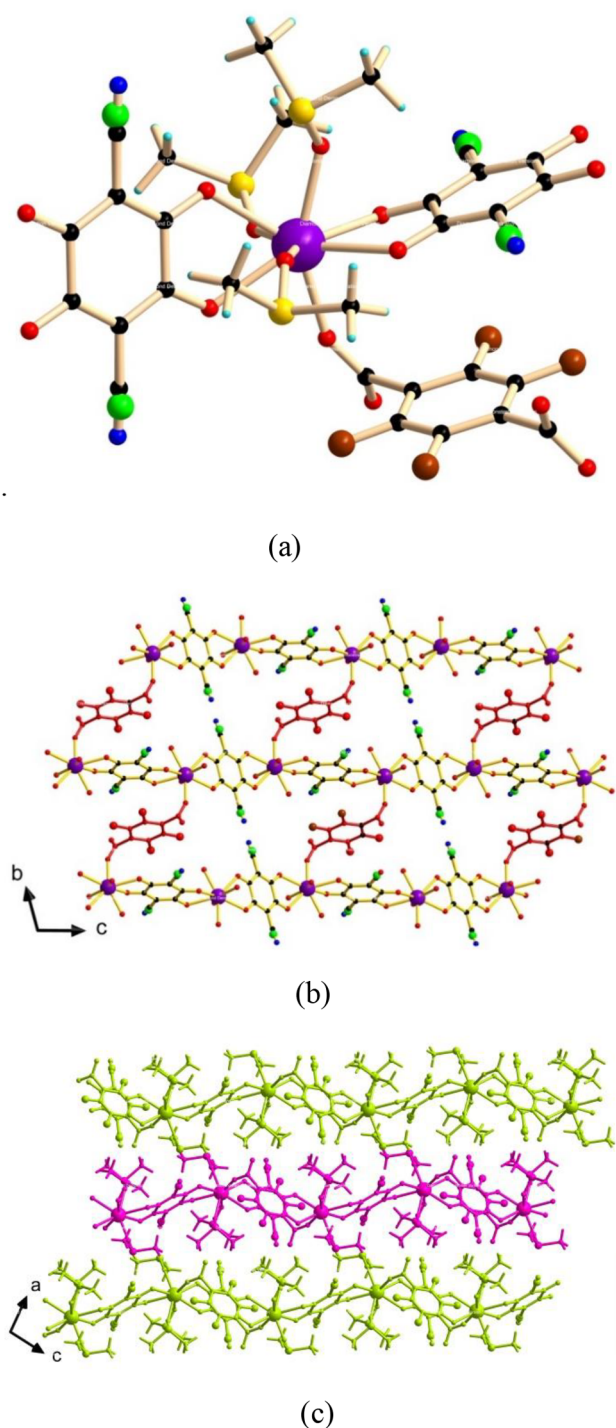
(a)

(b)

(c)

Figure 1. (a) Coordination environment around a Er^{III} metal ion. (b) View of the 2D layers in the *bc* plane, highlighting a second ligand in red. (c) View of the 2D layers in the *ac* plane. Neighboring layers are shown in different colors. Color code: Er, purple; S yellow; O red; Cl green; F, brown; C, black; N, blue; H, cyan.

1D chains, thus leading to 2D layers. The neighboring 2D layers are eclipsed in the *bc* plane, forming parallelogram-like cavities. In the *ac* plane, the 2D layers are arranged in a wavelike manner (Figure 1c). A similar structure was reported for the homologous heteroleptic CP with the Yb^{III} ion.[31]

2.2. Photophysical Studies. Finely ground crystals of freshly prepared **1** were studied by continuous-wave (cw)

absorption spectroscopy and photoluminescence (PL) spectroscopy under pulsed-laser irradiance in a weak excitation regime, where the response of **1** is linear in the irradiance over a wide range. The results of the optical and photophysical studies are summarized in Figure 2.

The diffuse-reflectance (DR) spectrum, acquired over a broad spectral range spanning through the visible and NIR, shows evidence of both ligand- and Er^{III}-centered absorption processes (Figure 2a). The absorption band in the visible clearly resembles that of the homoleptic Er(Yb)-ClCNAn CPs reported previously[30] and is thus ascribed to the ClCNAn^{2-} linkers. In the near-UV portion of the spectrum, below the 400 nm wavelength, the F$_4$BDC^{2-} ligands are expected to give a minority contribution to the optical absorption of **1**.[31] Dips observed between 1600 and 1800 nm were assigned to water absorption. PL spectra acquired separately in the 400−1100 and 1300−1800 nm wavelength ranges are, in fact, greatly complementary to the DR one (Figure 2a), making it easy to single out ligand (ClCNAn^{2-})-centered and Er^{III}-centered PL components. The emission band extending from 400 to 500 nm represents a background emission from the quartz substrates (see the Experimental Section); hence, F$_4$BDC^{2-} linkers appeared to be optically inactive overall, in line with their designed function as ancillary bridging units. Narrow peaks located at ∼540, ∼880, and ∼950 nm in the emission spectrum could not be identified and were attributed to residual room light.

As shown in Figure 2b, the ligand-centered emission triggered by the pulsed-laser pump exhibits fast monoexponential decay kinetics with a characteristic time of ∼40 ps, which is, in fact, close to the temporal resolution of the experiment. Because of the ∼200 ps PL lifetime of the ClCNAn^{2-} anion in the KHClCNAn salt, a strong excited-state relaxation channel was inferred to result from ligand coordination to Er^{III}. This was identified as a lanthanide-enhanced intersystem (singlet-to-triplet) crossing (ISC), which, following ligand-centered optical absorption, initiates the overall *antenna* effect, ending up with lanthanide sensitization.

The Er^{III}-centered ($^4I_{13/2} \rightarrow {}^4I_{15/2}$) emission band peaking at ∼1530 nm was found to rise in the time scale of a few tens of nanoseconds and decay in a few microseconds (Figure 2c,d). Curve fitting to the PL temporal profile was applied using a monoexponential rise and monoexponential decay function as follows:

$$I_{Er}(t) = A[\exp(-t/\tau_D) - \exp(-t/\tau_S)]$$
$$= A[1 - \exp(-t/\tau_R)]\exp(-t/\tau_D)$$

where A is the signal amplitude and τ_S, τ_R, and τ_D are the Er^{III}($^4I_{13/2}$) sensitization, rise, and decay time constants, respectively ($\tau_R^{-1} = \tau_S^{-1} - \tau_D^{-1}$). Curve fitting yielded $\tau_S = 20(1)$ ns and $\tau_D = 3.8(1)$ μs. Because the Er^{III}-centered emission sensitization process is much slower than the ClCNAn^{2-}-centered emission decay, cascaded energy relaxation from the ClCNAn^{2-} linkers to the Er^{III} ions through ISC and ligand-to-metal energy transfer is postulated to take place in **1**.[30,31]

The photophysical parameters of **1** and related compounds previously studied[30,31] are summarized in Table 1.

Noticeably, the observed Er^{III} NIR PL lifetime of 3.8 μs is almost twice as long as that of the corresponding homoleptic Er-ClCNAn CP (2.1 μs),[30] hinting to a possibly reduced vibrational quenching of the Er^{III} NIR emission in **1**. As a matter of fact, the first coordination sphere of Er^{III} in the homoleptic CP contains three DMF ligand molecules, bearing six −CH$_3$ groups and three
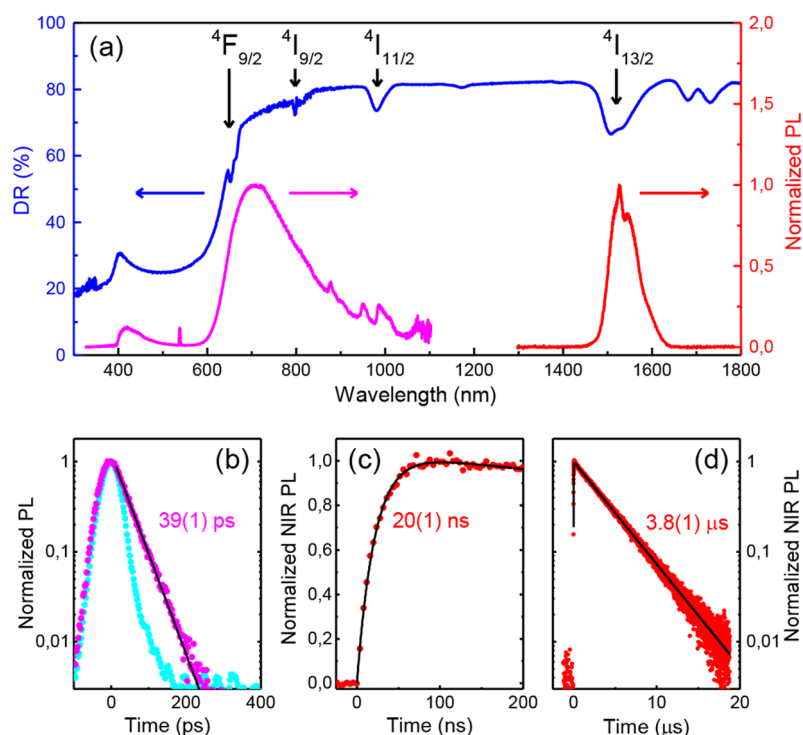
Figure 2. Optical and photophysical measurements on crystals of **1**. (a) DR spectrum (blue line, left scale) and PL spectra across the visible and NIR ranges under pulsed-laser irradiance at 355 nm (magenta and red lines, right scale). The spectroscopic terms of the upper states of Er^{III} absorption transitions are indicated. (b) Magenta dots: Time-resolved PL integrated over the ligand-centered band peaked at ~700 nm, showing the ligand excited-state decay. Black line: Best fit of a monoexponential decay curve to the data. Cyan dots: Impulse response function of the detection system. (c) Red dots: Time-resolved NIR PL integrated over the Er^{III} emission band peaked at 1530 nm, highlighting the lanthanide sensitization process. (d) Same as that in part c but on a much longer time range to display the lanthanide emission decay. The black lines in parts c and d represent the best fit of a two-component exponential function, modeling Er^{III} sensitization and decay kinetics, to the data (see the text for details). The sensitization and decay time constants are also shown in parts b–d.

Table 1. Ligand-Centered PL Decay Time (τ_L), Ln^{III}-Centered PL Sensitization time (τ_S), and Ln^{III}-Centered PL Decay Time (τ_D) of 1 and Compounds Investigated in Previous Work[30,31]

compound	reference	τ_L (ps)	τ_S (ns)	τ_D (μs)
[Er$_2$(ClCNAn)$_2$(F$_4$BDC)(DMSO)$_6$]$_n$ (**1**)	this work	39	20	3.8
{[Er$_2$(ClCNAn)$_3$(DMF)$_6$](DCM)$_2$}$_n$	30	42	16	2.1
[Yb$_2$(ClCNAn)$_3$(DMF)$_6$]$_n$	30	~30	<1	8.6
[Yb$_4$(ClCNAn)$_5$(DOBDC)(DMSO)$_{10}$]$_n$·(DMSO)$_2$	31	<30	<1	10
[Yb$_2$(ClCNAn)$_2$(F4BDC)(DMSO)$_6$]$_n$	31	<30	<1	3.8

197 −CH groups in total, whereas in **1**, the three coordinated
198 DMSO molecules contribute with only six −CH$_3$ groups. The
199 same qualitative considerations should, in principle, apply also
200 to the Yb-based CPs. In [Yb$_4$(ClCNAn)$_5$(DOBDC)-
201 (DMSO)$_{10}$]$_n$·(DMSO)$_2$, where the Yb^{III} coordination environ-
202 ment comprises, on average, five −CH$_3$ groups, one −CH group,
203 and one −OH group, a moderate increase in the NIR PL lifetime
204 was, in fact, reported with respect to the
205 [Yb$_2$(ClCNAn)$_3$(DMF)$_6$]$_n$ case. A corresponding improvement
206 in the NIR PL lifetime of Yb$_2$(ClCNAn)$_2$(F$_4$BDC)(DMSO)$_6$]$_n$
207 could, however, not be assessed, presumably because of a high
208 sensitivity of crystals of the F$_4$BDC-containing CP to ambient
209 conditions, actually resulting in a shorter lifetime.

210   **2.3. WFT Analysis.** In order to rationalize the luminescence
211 properties of the investigated complexes, multireference WFT

212 calculations were performed on the homoleptic CPs [Yb-
213 (ClCNAn)$_3$]$^{3-}$ and [Er(ClCNAn)$_3$]$^{3-}$ previously described[30]
214 and the heteroleptic [Er(ClCNAn)$_2$(F$_4$BDC)]$^{3-}$ as model
215 compounds (Figure 3; see the computational details). The
216 calculated energy-state diagrams at the restricted-active-space
217 self-consistent-field (RASSCF) level for these model com-
218 pounds are shown in Figures 4 and 5, while the numerical values
219 used for these diagrams are collected in Tables S1−S3.

220   At the spin-free (SF) level [i.e., without spin−orbit (SO)
221 coupling (SOC)], the excited ligand-centered singlet states S$_1$
222 are calculated at 636 (15711 cm^{-1}) and 646 nm (15483 cm^{-1}) in
223 [Yb(ClCNAn)$_3$]$^{3-}$ and [Er(ClCNAn)$_3$]$^{3-}$, respectively, and
224 compare very well with the experimental data of ca. 650 nm. As
225 illustrated by the natural orbitals (NOs) in Figures S2 and S3,
226 this first singlet excited state corresponds to a $\pi-\pi^*$ excitation
227 within the anilate ligands. In [Yb(ClCNAn)$_3$]$^{3-}$, the lowest
228 ligand-centered triplet state T$_1$ is located lower in energy than
229 the S$_1$ state (15297 vs 15711 cm^{-1}), while it is calculated at an
230 energy similar to that of the S$_1$ state in the Er^{III} analogue
231 compound (15577 vs 15483 cm^{-1}). Therefore, the calculated
232 gaps $\Delta E_{S_1-T_1}$ at the RASSCF level are of 414 and 94 cm^{-1} in the
233 ytterbium(III) and erbium(III) trianilate model compounds,
234 respectively, favoring a strong ISC between these states in both
235 complexes.

236   As as visible in Tables S1 and S2, the introduction of SOC
237 leads to a large admixture of the ligand-centered singlet and
238 triplet states into Kramers doublet (KD) states, which are
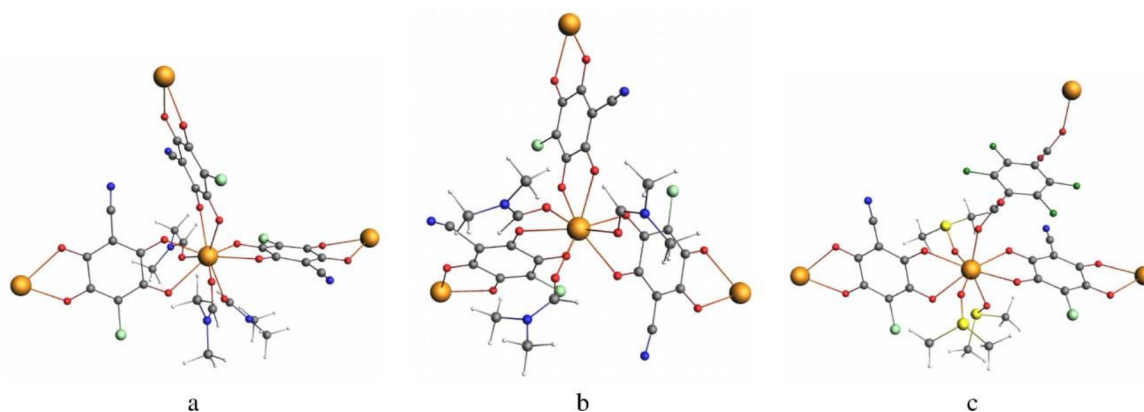239 labeled as the ISC area in Figures 4 and 5. Interestingly, in

Figure 3. Representations of the model compounds $[Yb(ClCNAn)_3]^{3-}$ (a), $[Er(ClCNAn)_3]^{3-}$ (b), and $[Er(ClCNAn)_2(F_4BDC)]^{3-}$ (c).

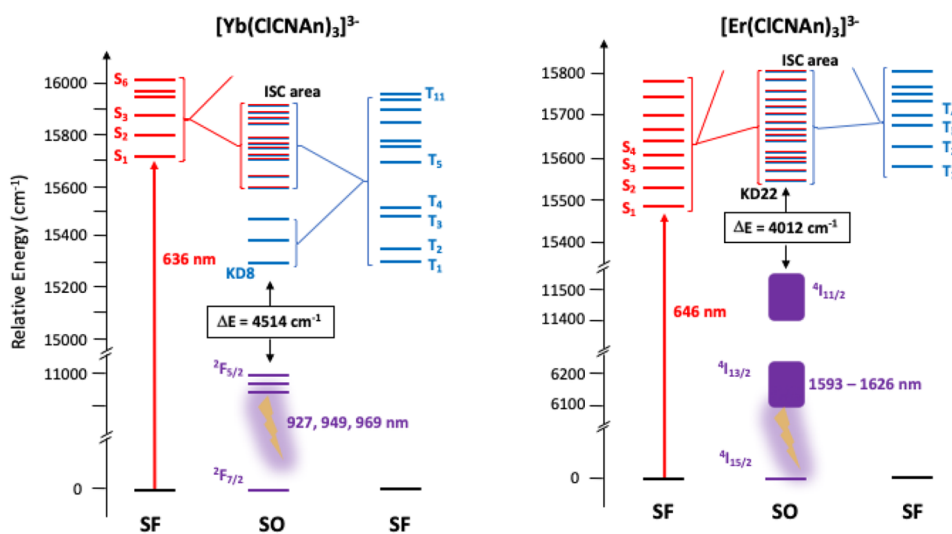**Figure 4.** Calculated energy-state diagrams (in cm^{-1}) of $[Yb(ClCNAn)_3]^{3-}$ (left) and $[Er(ClCNAn)_3]^{3-}$ (right). Note the change in the energy scale between the two state diagrams.

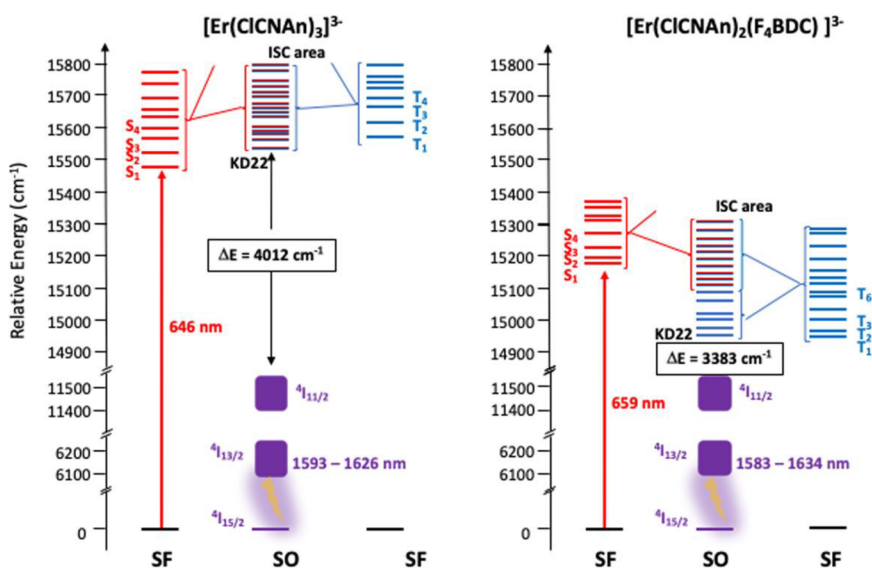**Figure 5.** Calculated energy-state diagrams (in cm^{-1}) of $[Er(ClCNAn)_3]^{3-}$ (left) and $[Er(ClCNAn)_2(F_4BDC)]^{3-}$ (right).

$[Yb(ClCNAn)_3]^{3-}$, a set of three KD states arising mainly from the SF triplet spin states are calculated below the ISC area and can thus participate in nonradiative relaxation processes. In both the ytterbium(III) and erbium(III) trianilate model com-

pounds, the ligand-centered KDs are located above the lanthanide emissive states. In $[Yb(ClCNAn)_3]^{3-}$, an energy gap of ca. 4500 cm^{-1} is calculated between the lowest KD states centered on the anilate ligands and the emissive KDs of the $^2F_{5/2}$ level, allowing efficient energy transfer. In agreement with the experimental data ($\lambda_{ems} \approx 980$ nm), the three emissive KDs are calculated as 10318, 10583, and 10784 cm^{-1}. In $[Er(ClCNAn)_3]^{3-}$, the lowest ligand-centered KD (KD22) is located at ca. 4000 cm^{-1} above the Er^{III}-centered excited states of the $^4I_{11/2}$ level. Here, the emissive KDs of the $^4I_{13/2}$ level are calculated between 6148 and 6276 cm^{-1}, slightly lower in energy than that in the experimental observation ($\lambda_{ems} \approx 1500-1570$ nm).

The influence of the substitution of one anilate ligand by a tetrafluoroterephthalate ligand in $[Er(ClCNAn)_2(F_4BDC)]^{3-}$ is shown in Figure 5 with the calculated state diagram. At the SF level, the comparison between the two state diagrams reveals a sizable energetic stabilization of the S_1 (311 cm^{-1}) and T_1 (634 cm^{-1}) states in $[Er(ClCNAn)_2(F_4BDC)]^{3-}$. This energetic stabilization of the lowest singlet and triplet states could arise from the ligand substitution but could also result from the difference in the choice of the active space and the number of roots included in the state-average calculations (see the computational details) and thus prevents a clear conclusion. Nevertheless, at the SO level, the ligand substitution barely influences the energy of the Er^{III}-centered states. For instance, the emissive states from the $^4I_{13/2}$ level are calculated between 6118 and 6316 cm^{-1} above the ground state in $[Er(ClCNAn)_2(F_4BDC)]^{3-}$, while the corresponding states in the trianilate compound were calculated between 6148 and 6276 cm^{-1}. Because of the energetic stabilization of the SF singlet and triplet states, the lowest ligand-centered KD in $[Er(ClCNAn)_2(F_4BDC)]^{3-}$ is marginally closer in energy to the Er^{III}-centered $^4I_{11/2}$ level ($\Delta E = 3383$ cm^{-1}) than to the trianilate analogue ($\Delta E = 4012$ cm^{-1}).

Through this theoretical study, the efficient antenna effect of the chlorocyananilate ligand in the sensitization of NIR-emissive lanthanide complexes, thanks to efficient energy transfer from KD states, is thus clearly demonstrated for the first time.

3. CONCLUSIONS

A combined experimental/theoretical study on the luminescent properties of homoleptic/heteroleptic erbium(III) anilate-based 2D CPs is herein reported. The heteroleptic neutral 2D CP, formulated as $[Er_2(ClCNAn)_2(F_4BDC)(DMSO)_6]_n$ (1), has been synthesized by combining Er^{III} ions with ClCNAn^{2-}/F$_4$BDC^{2-} linkers, via a one-pot synthetic strategy, and structurally characterized. Photophysical measurements emphasized the role of the chlorocyananilate linker as an optical *antenna* toward Er^{III} ions, as was already observed in previously reported homoleptic neutral 2D Yb^{III} and Er^{III} CPs. The remarkable increase observed in the Er^{III} NIR PL lifetime (3.8 μs), which was attributed to reduced vibrational quenching, points out the beneficial effect of the fully fluorinated F$_4$BDC^{2-} linker on the NIR emission efficiency of Er^{III}. WFT calculations demonstrate the dominant role of the chlorocyananilate linker as an optical *antenna* responsible for Er^{III} NIR luminescence sensitization, through efficient energy transfer from KD states. It is worth noting that this theoretical approach can provide guidelines for a rational design of Ln-CPs with efficient NIR emission, which can be modulated by the proper selection of a ligand admixture. It is also worth mentioning that Ln^{III}-based molecular materials have been increasingly considered in recent years for potential bioapplications using upconversion luminescence processes.[38,39] In the specific case of Er^{III}-based materials such as Er^{III} CPs, green upconversion luminescence for, e.g., bioimaging and photodynamic therapy, applications can be generated by Er^{III} direct photoexcitation using a convenient cw laser diode at 980 nm wavelength, in the optical transparency window, where the light penetration depth in the biological tissues can be of several centimeters.

4. EXPERIMENTAL SECTION

4.1. Materials and Methods. Reagents of analytical grade were purchased from Zentek (TCI) and used without further purification. The HPLC-grade solvents were purchased from Thermofisher Scientific Alfa-Aesar. KHClCNAn was synthesized as reported in the literature,[33] while Er(NO$_3$)$_3$·5H$_2$O and H$_2$F$_4$BDC were purchased from Thermofisher Scientific Alfa-Aesar and used without further purification.

4.2. Synthesis of $[Er_2(ClCNAn)_2(F_4BDC)(DMSO)_6]_n$ (1). The compound was synthesized by adapting our procedure,[31] using Er(NO$_3$)$_3$·5H$_2$O (230 mg, 0.6 mmol) instead of YbCl$_3$·5H$_2$O.

4.3. X-ray Crystallography. Single crystals of the compound were mounted on glass fiber loops using a viscous hydrocarbon oil to coat the crystal and then transferred directly to the cold nitrogen stream for data collection. Data collection was performed at 150 K on an Agilent Supernova with Cu Kα ($\lambda = 1.54184$ Å). The structures were solved by direct methods with the *SIR97* program and refined against all F^2 values with the *SHELXL-97* program using the *WinGX* graphical user interface. All non-H atoms were refined anisotropically except as noted, and H atoms were placed in calculated positions and refined isotropically with a riding model. A summary of the crystallographic data and structure refinement is given in Table 2.

4.4. Photophysical Characterization. cw DR of finely ground crystals of **1** was measured in a hemispherical geometry using a dual-

Table 2. Crystallographic Data of Compound 1

empirical formula	C$_{34}$H$_{36}$Cl$_2$Er$_2$F$_4$N$_2$O$_{18}$S$_6$
fw (g/mol)	1434.43
cryst color	red
cryst size (mm^3)	0.3 × 0.2 × 0.15
temperature (K)	150
wavelength (Å)	1.54184
cryst syst, Z	triclinic, 1
space group	P-1
a (Å)	9.1849(3)
b (Å)	9.7764(3)
c (Å)	14.8035(5)
α (deg)	103.718(3)
β (deg)	93.278(3)
γ (deg)	107.223(3)
V (Å^3)	1221.78(7)
ρ_{calc} (g/cm^3)	1.950
μ(Cu Kα) (mm^{-1})	10.361
θ range (deg)	3.102−73.339
data collected	8501
data unique	4724
data observed	4540
R(int)	0.0266
no. of param/restraints	334/15
$R_1(F)^a$ [$I > 2\sigma(I)$]	0.0282
$wR_2(F^2)^b$ (all data)	0.0717
$S(F^2)^c$ (all data)	1.107
CCDC	2101373

$^aR_1(F) = \sum ||F_o| - |F_c||/\sum|F_o|.$ $^bwR_2(F^2) = [\sum w(F_o^2 - F_c^2)^2/\sum wF_o^4]^{1/2}.$ $^cS(F^2) = [\sum w(F_o^2 - F_c^2)^2/(n + r - p)]^{1/2}.$

beam spectrophotometer with an integrating-sphere accessory (Agilent Cary 5000 UV−vis−NIR). PL experiments were performed with the sample crystals embedded between quartz slides, using a reflection geometry for signal collection. Ligand-centered PL was excited by an optical parametric amplifier (TOPAS-C Light Conversion) pumped by a regenerative Ti:sapphire amplifier (Coherent Libra-HE; 355 nm wavelength, ∼200 fs pulse duration, and 1 kHz pulse repetition frequency). PL detection was accomplished using a streak camera (Hamamatsu C10910) mounted on a grating spectrometer (Princeton Instruments Acton SpectraPro SP-2300), providing ∼30 ps temporal resolution. Ln-centered PL was photoexcited by a passively Q-switched powerchip laser (Teem Photonics PNV-M02510; 355 nm wavelength, ∼350 ps pulse duration, and 1 kHz pulse repetition frequency), spectrally analyzed using a grating spectrometer (Princeton Instruments Acton SpectraPro 2300i), and measured by a NIR array detector (Andor iDus InGaAs 1.7 μm) or a NIR photomultiplier (Hamamatsu H10330A-75) interfaced with a digital oscilloscope with a 1 GHz bandwidth (Tektronix TDS 5104).

4.5. Computational Details. The Amsterdam Density Functional (*ADF*)[40−42] software package was used to perform partial structural optimization on the X-ray structures of the investigated complexes. The positions of the H atoms were optimized by using Kohn−Sham density functional theory, whereas the rest of the atoms were kept frozen. These calculations utilized the scalar all-electron zeroth-order regular approximation,[43] and the spin-restricted formalism was employed by replacing the open-shell Er^{III} and Yb^{III} ions by closed-shell Y^{III} ones. The hybrid functional PBE0[44,45] (Perdew−Burke−Ernzerhof) with 25% exact exchange was employed along with the triple-ζ-polarized Slater-type orbital all-electron basis set with one set of polarization functions for all atoms (TZP).[46]

The multireference WFT calculations were performed with the help of the *OpenMolcas* software packages[47] on the model compounds shown in Figure 3. In these calculations, the RASSCF[48] approach was used to treat the static correlation effects. The second-order Douglas−Kroll−Hess[49−52] scalar-relativistic (SR) Hamiltonian was used to treat the SR effects in combination with the all-electron atomic natural orbital relativistically contracted basis set from the *Molcas* library.[53−55] The basis sets were contracted to TZP quality for the Er, Yb, and O atoms coordinated to the Ln center (Er and Yb, 25s22p15d11f4g2h/8s7p4d3f2g1h; O, 14s9p5d3f2g/4s3p2d1f), to the double-ζ plus polarization quality for the C, N, O, F, S, and Cl atoms (C, N, O, and F, 14s9p4d3f2g/3s2p1d; S and Cl, 17s12p5d4f2g/4s3p1d), and to the double-ζ quality for the H atoms (H, 8s4p3d1f/2s). Additionally, three surrounding Ln^{III} ions (Er^{III} or Yb^{III}) were described by zero-electron-charged ab initio model potentials.[56]

In $[Yb(ClCNAn)_3]^{3−}$, calculations were performed with a RAS-[19,1,1,3,7,3]SCF active space. This RASSCF calculation was done on top of a CAS(13,7)SCF wave function used to model the static correlation arising from the $4f^{13}$ Yb^{III} ion. The RASSCF calculation was allowed to create (i) one hole in the RAS1 space containing a doubly occupied bonding molecular orbital centered on the anilate ligands and (ii) one particle in the RAS3 space containing an unoccupied antibonding molecular orbital on the ligand (Figure S2). The calculations employed the state-averaged formalism at the SR level by taking into account 13 quartet spin states corresponding to the combinations of triplet spin states centered on the ligand fragment $(\pi-\pi^*)^3$ and doublet spin states of the Yb^{III} ion (^2F). Additionally, 24 doublet spin states were also considered that correspond to the combinations of singlet spin states of the anilate ligands $(\pi-\pi^*)^1$ and the ^2F doublet spin states of the metal center. In $[Er(ClCNAn)_3]^{3−}$, the calculations were performed with a RAS[17,1,1,3,7,3]SCF active space on top of a CAS(11,7)SCF wave function used to model the static correlation arising from the $4f^{11}$ Er^{III} ion. The state-average SR calculations were performed by taking into account 16 sextet spin states corresponding to the combinations of triplet spin states centered on the ligand fragment $(\pi-\pi^*)^3$ and quartet spin states of the Er^{III} ion (^4I). Additionally, 41 quartet and 112 doublet spin states were also considered that correspond to the combinations of singlet spin states of the anilate ligands $(\pi-\pi^*)^1$ and quartet and doublet spin states of the metal center. In $[Er(ClCNAn)_2(F_4BDC)]^{3−}$, calculations were

performed with a RAS[15,1,1,2,7,2]SCF active space on top of a CAS(11,7)SCF wave function used to model the static correlation arising from the $4f^{11}$ Er^{III} ion. Only two bonding and two antibonding orbitals centered on the anilate ligands were added in the RAS1 and RAS3 space, respectively (Figure S4). The state-average SR calculations were performed by taking into account 26 sextet, 41 quartet, and 112 doublet spin states.

SOC was then introduced within a state interaction among the basis set of calculated SR states using the restricted-active-space state interaction approach.[56] Herein the SOC matrix is diagonalized using the calculated SR spin states. The nature of the molecular orbital was then analyzed using NOs that were directly obtained from the multiconfigurational wave functions that include SOC effects. The procedure to obtain these orbitals is explained in refs 57−59. The orbitals were then visualized with the graphical interface of the *ADF* software package.

■ ASSOCIATED CONTENT

■ AUTHOR INFORMATION

Corresponding Authors

Narcis Avarvari − *MOLTECH-Anjou, Université Angers, CNRS, SFR MATRIX, Angers F-49000, France;* ⊚ orcid.org/0000-0001-9970-4494; Phone: (+33)02 41 73 50 84; Email: narcis.avarvari@univ-angers.fr; Fax: (+33)02 41 73 5405

Maria Laura Mercuri − *Dipartimento di Scienze Chimiche e Geologiche, Università degli Studi di Cagliari, Monserrato, Cagliari I-09042, Italy; Consorzio Interuniversitario Nazionale per La Scienza e Tecnologia Dei Materiali (INSTM), Firenze 50121, Italy;* ⊚ orcid.org/0000-0002-4816-427X; Phone: (+39)0706754486; Email: mercuri@unica.it; Fax: (+39)0706754486

Authors

Suchithra Ashoka Sahadevan − *Dipartimento di Scienze Chimiche e Geologiche, Università degli Studi di Cagliari, Monserrato, Cagliari I-09042, Italy; MOLTECH-Anjou, Université Angers, CNRS, SFR MATRIX, Angers F-49000, France;* Present Address: Department of Applied Physical Chemistry, KTH Royal Institute of Technology, SE-10044 Stockholm, Sweden

Fabio Manna − *Dipartimento di Scienze Chimiche e Geologiche, Università degli Studi di Cagliari, Monserrato, Cagliari I-09042, Italy*

Alexandre Abhervé − *MOLTECH-Anjou, Université Angers, CNRS, SFR MATRIX, Angers F-49000, France*

Mariangela Oggianu − *Dipartimento di Scienze Chimiche e Geologiche, Università degli Studi di Cagliari, Monserrato, Cagliari I-09042, Italy; Consorzio Interuniversitario Nazionale per La Scienza e Tecnologia Dei Materiali (INSTM), Firenze 50121, Italy*

Noemi Monni − *Dipartimento di Scienze Chimiche e Geologiche, Università degli Studi di Cagliari, Monserrato, Cagliari I-09042, Italy; Consorzio Interuniversitario Nazionale per La Scienza e Tecnologia Dei Materiali (INSTM), Firenze 50121, Italy*

Valentina Mameli − *Dipartimento di Scienze Chimiche e Geologiche, Università degli Studi di Cagliari, Monserrato, Cagliari I-09042, Italy; Consorzio Interuniversitario Nazionale per La Scienza e Tecnologia Dei Materiali (INSTM), Firenze 50121, Italy;* orcid.org/0000-0002-1899-8636

Daniela Marongiu − *Dipartimento di Fisica, Università degli Studi di Cagliari, Monserrato, Cagliari I-09042, Italy;* orcid.org/0000-0001-7085-769X

Francesco Quochi − *Dipartimento di Fisica, Università degli Studi di Cagliari, Monserrato, Cagliari I-09042, Italy; Consorzio Interuniversitario Nazionale per La Scienza e Tecnologia Dei Materiali (INSTM), Firenze 50121, Italy*

Frédéric Gendron − *Institut des Sciences Chimiques de Rennes, Université Rennes, CNRS, UMR 6226, Rennes 35000, France;* orcid.org/0000-0002-1896-3978

Boris Le Guennic − *Institut des Sciences Chimiques de Rennes, Université Rennes, CNRS, UMR 6226, Rennes 35000, France;* orcid.org/0000-0003-3013-0546

Complete contact information is available at:
https://pubs.acs.org/10.1021/acs.inorgchem.1c02386

Notes

The authors declare no competing financial interest.

■ REFERENCES

(1) Rocha, J.; Carlos, L. D.; Paz, F. A. A.; Ananias, D. Luminescent Multifunctional Lanthanides-Based Metal−Organic Frameworks. *Chem. Soc. Rev.* **2011**, *40*, 926−940.

(2) Cui, Y.; Yue, Y.; Qian, G.; Chen, B. Luminescent Functional Metal-Organic Frameworks. *Chem. Rev.* **2012**, *112*, 1126−1162.

(3) Hasegawa, Y.; Nakanishi, T. Luminescent Lanthanide Coordination Polymers for Photonic Applications. *RSC Adv.* **2015**, *5*, 338−353.

(4) Eliseeva, S. V.; Bünzli, J. C. G. Lanthanide Luminescence for Functional Materials and Bio-Sciences. *Chem. Soc. Rev.* **2010**, *39*, 189−227.

(5) Bünzli, J.-C. G.; Eliseeva, S. V. Intriguing Aspects of Lanthanide Luminescence. *Chem. Sci.* **2013**, *4*, 1939.

(6) Einkauf, J. D.; Clark, J. M.; Paulive, A.; Tanner, G. P.; De Lill, D. T. A General Model of Sensitized Luminescence in Lanthanide-Based Coordination Polymers and Metal-Organic Framework Materials. *Inorg. Chem.* **2017**, *56*, 5544−5552.

(7) Chatenever, A. R. K.; Warne, L. R.; Matsuoka, J. E.; Wang, S. J.; Reinheimer, E. W.; Lemagueres, P.; Fei, H.; Song, X.; Oliver, S. R. J. Isomorphous Lanthanide Metal-Organic Frameworks Based on Biphenyldicarboxylate: Synthesis, Structure, and Photoluminescent Properties. *Cryst. Growth Des.* **2019**, *19*, 4854−4859.

(8) Huang, J. J.; Yu, J. H.; Bai, F. Q.; Xu, J. Q. White-Light-Emitting Materials and Highly Sensitive Detection of Fe3+ and Polychlorinated Benzenes Based on Ln-Metal-Organic Frameworks. *Cryst. Growth Des.* **2018**, *18*, 5353−5364.

(9) Huang, W.; Pan, F.; Liu, Y.; Huang, S.; Li, Y.; Yong, J.; Li, Y.; Kirillov, A. M.; Wu, D. An Efficient Blue-Emissive Metal-Organic Framework (MOF) for Lanthanide-Encapsulated Multicolor and Stimuli-Responsive Luminescence. *Inorg. Chem.* **2017**, *56*, 6362−6370.

(10) Liu, L. H.; Qiu, X. T.; Wang, Y. J.; Shi, Q.; Sun, Y. Q.; Chen, Y. P. NIR Emission and Luminescent Sensing of a Lanthanide-Organic Framework with Lewis Basic Imidazole and Pyridyl Sites. *Dalton Trans.* **2017**, *46*, 12106−12113.

(11) Zhang, X.; Bing, Y.; Gao, P.; Bai, H.; Hu, M. High Sensitive Luminescent Sensing for Nitrobenzene and Iron(III) by Uncommon Ln-MOFs Containing Open Ketone Group Sites. *Inorg. Chim. Acta* **2017**, *455*, 98−104.

(12) Dang, S.; Yu, J. B.; Wang, X. F.; Guo, Z. Y.; Sun, L. N.; Deng, R. P.; Feng, J.; Fan, W. Q.; Zhang, H. J. A Study on the NIR-Luminescence Emitted from Ternary Lanthanide [Er(III), Nd(III) and Yb(III)] Complexes Containing Fluorinated-Ligand and 4,5-Diazafluoren-9-One. *J. Photochem. Photobiol., A* **2010**, *214*, 152−160.

(13) Yang, H. W.; Xu, P.; Ding, B.; Wang, X. G.; Liu, Z. Y.; Zhao, H. K.; Zhao, X. J.; Yang, E. C. Isostructural Lanthanide Coordination Polymers with High Photoluminescent Quantum Yields by Effective Ligand Combination: Crystal Structures, Photophysical Characterizations, Biologically Relevant Molecular Sensing, and Anti-Counterfeiting Ink Application. *Cryst. Growth Des.* **2020**, *20*, 7615−7625.

(14) Chen, B.; Yang, Y.; Zapata, F.; Qian, G.; Luo, Y.; Zhang, J.; Lobkovsky, E. B. Enhanced Near-Infrared-Luminescence in an Erbium Tetrafluoroterephthalate Framework. *Inorg. Chem.* **2006**, *45*, 8882−8886.

(15) Santos, J. C. C.; Pramudya, Y.; Krstić, M.; Chen, D. H.; Neumeier, B. L.; Feldmann, C.; Wenzel, W.; Redel, E. Halogenated Terephthalic Acid "Antenna Effects" in Lanthanide-SURMOF Thin Films. *ACS Appl. Mater. Interfaces* **2020**, *12*, 52166−52174.

(16) Mercuri, M. L.; Congiu, F.; Concas, G.; Sahadevan, S. A. Recent Advances on Anilato-Based Molecular Materials with Magnetic and/or Conducting Properties. *Magnetochemistry* **2017**, *3*, 17.

(17) Kitagawa, S. Coordination Compounds of 1,4-Dihydroxybenzoquinone and Its Homologues. Structures and Properties. *Coord. Chem. Rev.* **2002**, *224*, 11−34.

(18) Atzori, M.; Artizzu, F.; Sessini, E.; Marchiò, L.; Loche, D.; Serpe, A.; Deplano, P.; Concas, G.; Pop, F.; Avarvari, N.; Mercuri, M. L. Halogen-Bonding in a New Family of Tris(Haloanilato)Metallate(III) Magnetic Molecular Building Blocks. *Dalton Trans.* **2014**, *43*, 7006−7019.

(19) Atzori, M.; Pop, F.; Cauchy, T.; Mercuri, M. L.; Avarvari, N. Thiophene-Benzoquinones: Synthesis, Crystal Structures and Preliminary Coordination Chemistry of Derived Anilate Ligands. *Org. Biomol. Chem.* **2014**, *12*, 8752−8763.

(20) Sahadevan, S. A.; Abhervé, A.; Monni, N.; Sáenz de Pipaón, C.; Galán-Mascarós, J. R.; Waerenborgh, J. C.; Vieira, B. J. C.; Auban-Senzier, P.; Pillet, S.; Bendeif, E.-E.; Alemany, P.; Canadell, E.; Mercuri, M. L.; Avarvari, N. Conducting Anilate-Based Mixed-Valence Fe(II)-Fe(III) Coordination Polymer: Small-Polaron Hopping Model for Oxalate-Type Fe(II)Fe(III) 2D Networks. *J. Am. Chem. Soc.* **2018**, *140*, 12611−12621.

(21) Sahadevan, S. A.; Monni, N.; Abhervé, A.; Cosquer, G.; Oggianu, M.; Ennas, G.; Yamashita, M.; Avarvari, N.; Mercuri, M. L. Dysprosium Chlorocyanoanilate-Based 2D-Layered Coordination Polymers. *Inorg. Chem.* **2019**, *58*, 13988−13998.

(22) Abhervé, A.; Clemente-León, M.; Coronado, E.; Gómez-García, C. J.; Verneret, M. One-Dimensional and Two-Dimensional Anilate-Based Magnets with Inserted Spin-Crossover Complexes. *Inorg. Chem.* **2014**, *53*, 12014−12026.

(23) Benmansour, S.; Abhervé, A.; Gómez-Claramunt, P.; Vallés-García, C.; Gómez-García, C. J. Nanosheets of Two-Dimensional Magnetic and Conducting Fe(II)/Fe(III) Mixed-Valence Metal-Organic Frameworks. *ACS Appl. Mater. Interfaces* **2017**, *9*, 26210−26218.

(24) Jeon, I.-R.; Negru, B.; Van Duyne, R. P.; Harris, T. D. A 2D Semiquinone Radical-Containing Microporous Magnet with Solvent-Induced Switching from T c = 26 to 80 K. *J. Am. Chem. Soc.* **2015**, *137*, 15699−15702.

(25) DeGayner, J. A.; Jeon, I.-R.; Sun, L.; Dincă, M.; Harris, T. D. 2D Conductive Iron-Quinoid Magnets Ordering up to Tc = 105 K via Heterogenous Redox Chemistry. *J. Am. Chem. Soc.* **2017**, *139*, 4175−4184.

(26) Sahadevan, S. A.; Abhervé, A.; Monni, N.; Auban-Senzier, P.; Cano, J.; Lloret, F.; Julve, M.; Cui, H.; Kato, R.; Canadell, E.; Mercuri, M. L.; Avarvari, N. Magnetic Molecular Conductors Based on Bis(Ethylenedithio)Tetrathiafulvalene (BEDT-TTF) and the Tris-(Chlorocyananilato)Ferrate(III) Complex. *Inorg. Chem.* **2019**, *58*, 15359−15370.

(27) Ashoka Sahadevan, S.; Monni, N.; Abhervé, A.; Auban-Senzier, P.; Canadell, E.; Mercuri, M. L.; Avarvari, N. Synthesis and Physical Properties of Purely Organic BEDT-TTF-Based Conductors Containing Hetero-/Homosubstituted Cl/CN-Anilate Derivatives. *Inorg. Chem.* **2017**, *56*, 12564−12571.

(28) Atzori, M.; Pop, F.; Auban-Senzier, P.; Clérac, R.; Canadell, E.; Mercuri, M. L.; Avarvari, N. Complete Series of Chiral Paramagnetic Molecular Conductors Based on Tetramethyl-Bis(Ethylenedithio)-Tetrathiafulvalene (TM-BEDT-TTF) and Chloranilate-Bridged Heterobimetallic Honeycomb Layers. *Inorg. Chem.* **2015**, *54*, 3643−3653.

(29) Atzori, M.; Pop, F.; Auban-Senzier, P.; Gómez-García, C. J.; Canadell, E.; Artizzu, F.; Serpe, A.; Deplano, P.; Avarvari, N.; Mercuri, M. L. Structural Diversity and Physical Properties of Paramagnetic Molecular Conductors Based on Bis(Ethylenedithio)-Tetrathiafulvalene (BEDT-TTF) and the Tris(Chloranilato)Ferrate-(III) Complex. *Inorg. Chem.* **2014**, *53*, 7028−7039.

(30) Ashoka Sahadevan, S.; Monni, N.; Abhervé, A.; Marongiu, D.; Sarritzu, V.; Sestu, N.; Saba, M.; Mura, A.; Bongiovanni, G.; Cannas, C.; Quochi, F.; Avarvari, N.; Mercuri, M. L. Nanosheets of Two-Dimensional Neutral Coordination Polymers Based on Near-Infrared-Emitting Lanthanides and a Chlorocyananilate Ligand. *Chem. Mater.* **2018**, *30*, 6575−6586.

(31) Ashoka Sahadevan, S.; Monni, N.; Oggianu, M.; Abhervé, A.; Marongiu, D.; Saba, M.; Mura, A.; Bongiovanni, G.; Mameli, V.; Cannas, C.; Avarvari, N.; Quochi, F.; Mercuri, M. L. Heteroleptic NIR-Emitting Yb^{III}/Anilate-Based Neutral Coordination Polymer Nanosheets for Solvent Sensing. *ACS Appl. Nano Mater.* **2020**, *3*, 94−104.

(32) Benmansour, S.; Pérez-Herráez, I.; López-Martínez, G.; Gómez-García, C. J. Solvent-Modulated Structures in Anilato-Based 2D Coordination Polymers. *Polyhedron* **2017**, *135*, 17−25.

(33) Atzori, M.; Artizzu, F.; Marchiò, L.; Loche, D.; Caneschi, A.; Serpe, A.; Deplano, P.; Avarvari, N.; Mercuri, M. L. Switching-on Luminescence in Anilate-Based Molecular Materials. *Dalton Trans.* **2015**, *44*, 15786−15802.

(34) Zheng, Z.; Lu, H.; Wang, Y.; Bao, H.; Li, Z. J.; Xiao, G. P.; Lin, J.; Qian, Y.; Wang, J. Q. Tuning of the Network Dimensionality and Photoluminescent Properties in Homo- And Heteroleptic Lanthanide Coordination Polymers. *Inorg. Chem.* **2021**, *60*, 1359−1366.

(35) Jin, G. Q.; Ning, Y.; Geng, J. X.; Jiang, Z. F.; Wang, Y.; Zhang, J. L. Joining the Journey to near Infrared (NIR) Imaging: The Emerging Role of Lanthanides in the Designing of Molecular Probes. *Inorg. Chem. Front.* **2020**, *7*, 289−299.

(36) Yu, H. H.; Li, J.; Yang, Y.; Li, X.; Su, Z. M.; Sun, J. Near-Infrared (NIR-II) Luminescence for the Detection of Cyclotetramethylene Tetranitramine Based on Stable Nd-MOF. *J. Solid State Chem.* **2021**, *294*, 121789.

(37) Gómez-Claramunt, P.; Benmansour, S.; Hernández-Paredes, A.; Cerezo-Navarrete, C.; Rodríguez-Fernández, C.; Canet-Ferrer, J.; Cantarero, A.; Gómez-García, C. J. Tuning the Structure and Properties of Lanthanoid Coordination Polymers with an Asymmetric Anilato Ligand. *Magnetochemistry* **2018**, *4*, 6.

(38) Li, M.; Gul, S.; Tian, D.; Zhou, E.; Wang, Y.; Han, Y.; Yin, L.; Huang, L. Erbium(III)-Based Metal−Organic Frameworks with Tunable Upconversion Emissions. *Dalton Trans.* **2018**, *47*, 12868−12872.

(39) Zhang, X.; Li, B.; Ma, H.; Zhang, L.; Zhao, H. Metal−Organic Frameworks Modulated by Doping Er^{3+} for Up-conversion Luminescence. *ACS Appl. Mater. Interfaces* **2016**, *8*, 17389−17394.

(40) te Velde, G.; Bickelhaupt, F. M.; Baerends, E. J.; van Gisbergen, S. J. A.; Fonseca Guerra, C.; Snijders, J. G.; Ziegler, T. Chemistry with ADF. *J. Comput. Chem.* **2001**, *22*, 931−967.

(41) Fonseca Guerra, C.; Snijders, J. G.; te Velde, G.; Baerends, E. J. Towards an Order-N DFT Method. *Theor. Chem. Acc.* **1998**, *99*, 391.

(42) Baerends, E. J.; Ziegler, T.; Atkins, A. J.; Autschbach, J.; Bashford, D.; Baseggio, O.; Bérces, A.; Bickelhaupt, F. M.; Bo, C.; Boerritger, P. M.; Cavallo, L.; Daul, C.; Chong, D. P.; Chulhai, D. V.; Deng, L.; Dickson, R. M.; Dieterich, J. M.; Ellis, D. A. L. *ADF2017, SCM, Theoretical Chemistry*; Vrije Universiteit: Amsterdam, The Netherlands, 2017.

(43) van Lenthe, E.; Baerends, E. J.; Snijders, J. G. Relativistic Regular Two-Component Hamiltonians. *J. Chem. Phys.* **1993**, *99*, 4597−4610.

(44) Adamo, C.; Barone, V. Toward Reliable Density Functional Methods without Adjustable Paramaters: The PBE0Model. *J. Chem. Phys.* **1999**, *110*, 6158−6170.

(45) Ernzerhof, M.; Scuseria, G. E. Assessment of the Perdew-Burke-Ernzerhof Exchange-Correlation Funtional. *J. Chem. Phys.* **1999**, *110*, 5029−5036.

(46) van Lenthe, E.; Baerends, E. J. Optimized Slater-Type Basis Sets for the Elements 1 − 118. *J. Comput. Chem.* **2003**, *24*, 1142−1156.

(47) Fdez. Galván, I.; Vacher, M.; Alavi, A.; Angeli, C.; Aquilante, F.; Autschbach, J.; Bao, J. J.; Bokarev, S. I.; Bogdanov, N. A.; Carlson, R. K.; Chibotaru, L. F.; Creutzberg, J.; Dattani, N.; Delcey, M. G.; Dong, S. S.; Dreuw, A.; Freitag, L.; Frutos, L. R.; et al. OpenMolcas: From Source Code to Insight. *J. Chem. Theory Comput.* **2019**, *15*, 5925−5964.

(48) Roos, B. O.; Taylor, P. R.; Sigbahn, P. E. M. A Complete Active Space SCF Method (CASSCF) Using a Density Matrix Formulated Super-CI Approach. *Chem. Phys.* **1980**, *48*, 157−173.

(49) Douglas, M.; Kroll, N. M. Quantum Electrodynamical Corrections to the Fine Structure of Helium. *Ann. Phys.* **1974**, *82*, 89−155.

(50) Hess, B. A. Applicability of the No-Pair Equation with Free-Particle Projection Operators to Atomic and Molecular Structure Calculations. *Phys. Rev. A: At., Mol., Opt. Phys.* **1985**, *32*, 756−763.

(51) Hess, B. A. Relativistic Electronic-Structure Calculations Employing a Two-Component No-Pair Formalism with External-Field Projection Operators. *Phys. Rev. A: At., Mol., Opt. Phys.* **1986**, *33*, 3742−3748.

(52) Wolf, A.; Reiher, M.; Hess, B. A. The Generalized Douglas-Kroll Transformation. *J. Chem. Phys.* **2002**, *117*, 9215−9226.

(53) Widmark, P.-O.; Malmqvist, P.-Å.; Roos, B. O. Density-Matrix Averaged Atomic Natural Orbital (ANO) Basis-Sets for Correlated Molecular Wave-Functions. I. First Row Atoms. *Theor. Chim. Acta* **1990**, *77*, 291−306.

(54) Roos, B. O.; Lindh, R.; Malmqvist, P.-Å.; Veryazov, V.; Widmark, P.-O. Main Group Atoms and Dimers Studied with a New Relativistic ANO Basis Set. *J. Phys. Chem. A* **2004**, *108*, 2851−2858.

(55) Roos, B. O.; Lindh, R.; Malmqvist, P.-Å.; Veryazov, V.; Widmark, P.-O. New Relativistic ANO Basis Sets for Transition Metal Atoms. *J. Phys. Chem. A* **2005**, *109*, 6575.

(56) Malmqvist, P.-A.; Roos, B. O.; Schimmelpfennig, B. The Restricted Active Space (RAS) State Interaction Approach with Spin-Orbit Coupling. *Chem. Phys. Lett.* **2002**, *357*, 230−240.

(57) Gendron, F.; Páez-Hernández, D.; Notter, F.-P.; Pritchard, B.; Bolvin, H.; Autschbach, J. Magnetic Properties and Electronic Structure of Neptunyl(VI) Complexes: Wavefunctions, Orbitals, and Crystal-Field Models. *Chem. - Eur. J.* **2014**, *20*, 7994−8011.

(58) Gendron, F.; Pritchard, B.; Bolvin, H.; Autschbach, J. Single-Ion 4f Element Magnetism: An Ab-Initio Look at Ln(COT)2-. *Dalton Trans.* **2015**, *44*, 19886−19900.

(59) Autschbach, J. Orbitals for Analyzing Bonding and Magnetism of Heavy-Metal Complexes. *Comments Inorg. Chem.* **2016**, *36*, 215−244.